CrossMark

Optimization of *in vivo* DNA delivery with NickFect peptide vectors

Krista Freimann [a,*], Piret Arukuusk [a], Kaido Kurrikoff [a], Luís Daniel Ferreira Vasconcelos [b], Kadi-Liis Veiman [a], Julia Uusna [a], Helerin Margus [c], Alfonso T. Garcia-Sosa [d], Margus Pooga [c], Ülo Langel [a,b]

[a] Laboratory of Molecular Biotechnology, Institute of Technology, University of Tartu, Nooruse, 50411 Tartu, Estonia
[b] Department of Neurochemistry, The Arrhenius Laboratories for Natural Sciences, Stockholm University, SE-10691 Stockholm, Sweden
[c] Department of Developmental Biology, Institute of Molecular and Cell Biology, University of Tartu, Riia 23, 51010 Tartu, Estonia
[d] Institute of Chemistry, University of Tartu, Ravila 14a, 50411 Tartu, Estonia

ABSTRACT

As the field of gene therapy progresses, an increasingly urgent need has arisen for efficient and non-toxic vectors for the *in vivo* delivery of nucleic acids. Cell-penetrating peptides (CPP) are very efficient transfection reagents *in vitro,* however, their application *in vivo* needs improvement.
To enhance *in vivo* transfection we designed various CPPs based on previous knowledge of internalization studies and physiochemical properties of NickFect (NF) nanoparticles. We show that increment of the helicity of these Transportan10 analogues improves the transfection efficiency. We rationally design by modifying the net charge and the helicity of the CPP a novel amphipathic α-helical peptide NF55 for *in vivo* application. NF55 condenses DNA into stable nanoparticles that are resistant to protease degradation, promotes endosomal escape, and transfects the majority of cells in a large cell population.
We demonstrate that NF55 mediates DNA delivery *in vivo* with gene induction efficiency that is comparable to commercial transfection reagents. In addition to gene induction in healthy mice, NF55/DNA nanoparticles showed promising tumor transfection in various mouse tumor models, including an intracranial glioblastoma model. The efficiency of NF55 to convey DNA specifically into tumor tissue increased even further after coupling a PEG2000 to the peptide *via* a disulfide-bond. Furthermore, a solid formulation of NF55/DNA displayed an excellent stability profile without additives or special storage conditions.
Together, its high transfection efficacy and stability profile make NF55 an excellent vector for the delivery of DNA *in vivo*.

© 2016 Elsevier B.V. All rights reserved.

1. Introduction

In recent decades, important advances have been achieved in genomics and gene-based therapies which have provided a range of new targets for genetic medicine. Now, almost any sequence in both the genome and the transcriptome has the potential to be regulated for therapeutic purposes through the introduction of exogenous nucleic acids into cells [1]. Therefore, gene therapy has been widely utilized to the development of antineoplastic drugs and approximately two-thirds of the clinical trials in gene therapy have aimed to treat various types of cancer [2]. Despite significant progress in the development of therapeutic nucleic acids, their use is still hindered by a low cellular uptake caused by poor cell membrane permeability [3]. As a result, a fundamental challenge to create effective gene-based therapies is the development of safe, selective targeting and delivery of nucleic acids.

Cell-penetrating peptides (CPPs) have been utilized for both the *in vitro* and *in vivo* delivery of various types of molecules, including small drug molecules, proteins and nucleic acid-based macromolecules. [4,5] CPPs are short peptides (around 30 residues) that have the capacity to cross cellular membranes with very limited toxicity. They are good alternatives to viral vectors, which have many limitations such as possible carcinogenesis, immunogenicity, and a limited capacity to package DNA. [6–8].

We have previously designed very efficient stearylated Transportan (TP) analogues termed NickFects for *in vitro* application [9–12]. TP10 is an amphipathic CPP with a net positive charge of +5 at physiological pH and is known to adopt an α-helical secondary structure. [13,14] Multiple studies have shown both the importance of charge and amphipathicity on the peptide transfection efficiency [6,15–17]. Moreover, increasing the secondary amphipathicity of the peptide has been shown to enhance gene delivery with many different CPPs. [15,16,18] Sharma et al. and Rajpal et al. have increased the secondary amphipathicity and/or the total charge of the CPPs and thereby enhanced transfection [15,16]. In addition, Song et al. have demonstrated that replacement of Lys with Arg in the TP10 sequence significantly

decreases its cell penetrating activity, which may be explained by the change in amphipathicity of the peptide [19]. Therefore, we hypothesized that further modification of the amphipathic properties and total charge of NickFects could improve their transfection efficacy.

CPPs have been utilized mostly *in vitro* and although many CPPs have been specifically designed for *in vivo* applications their transfection ability still needs improvement. This is supported by the fact that around 70% of gene therapy clinical trials carried out to date have used viral vectors [1]. Therefore, our aim here was to design more useable and efficient *in vivo* transfection vectors.

In this study, we rationally designed a new CPP NF55 based on previous knowledge of the physiochemical properties of NF/pDNA particles together with internalization studies. Herein, we characterize NF55/pDNA particles and demonstrate that they are able to effectively transfect cells with pDNA both *in vitro* and *in vivo*.

2. Methods

2.1. Peptide synthesis

Peptides were synthesized, cleaved from resin and purified as described previously [11]. For PEGylated peptides Boc-Cys(Npys)-OH was coupled to PEG2000. In NF551 Boc-l-Lys(Mtt)-OH was used and the protecting group was selectively removed with 0.1% TFA and Cys was attached *via* ε-amino group of Lys13. In NF552 Cys was coupled to the C-terminus of the peptide. Thereafter, Cys(Npys)-PEG2000 and peptide were incubated at pH 7.4 in PBS overnight.

LogP of peptides were calculated using Marvin Sketch64.

2.2. Computational methods

Structures of individual peptides were built or adapted from elsewhere [20], and minimized in implicit solvent using Schrödinger Software Package version 2015. For the resulting structures, the molecular surfaces, molecular electrostatic potentials, and hydrophilic/hydrophobic maps were calculated with Maestro. [21] Primary sequences of standard amino acids were used to calculate the potential for aggregation using statistical mechanics in Tango. [22]

2.3. Circular dichroism

Circular dichroism spectroscopy was used to determine the secondary structure of the peptides. CD spectra were recorded on a Chirascan CD spectrometer (Applied Photophysics, Leatherhead, UK) at 20 °C. Peptides were dissolved in MiliQ H_2O at 2 μM. Signal was recorded for a wavelength interval between 190 nm and 260 nm, using a bandwidth of 0.5 nm. A quartz cuvette (Hellma Analytics, Germany) with an optical path length of 1 mm was used, which required approximately 300 μl of sample. The temperature was adjusted to 20 °C using a TC 125 temperature controller. The background spectrum of the solvent was subtracted from all spectra. Spectra were collected, smoothened and averaged over 10 measurements. Conversion from CD units (mdeg) to Mean Residue Ellipticity (deg·cm²·dmol⁻¹) was done using the conversion tool from Pro-Data™ software (Applied Photophysics, Leatherhead, UK). Estimation of α helix and β strand content of the peptides, from their circular dichroism spectra, was calculated using the K2D2 algorythm. [23]

2.4. Complex formation

For complex formation, stability and cell culture assays NF/pDNA nanoparticles were prepared as described previously [11,24]. Briefly 0.25 μg of luciferase expressing plasmid (pLuc2) was mixed with NFs at charge ratio (CR) 1 to 4 in MilliQ water and incubated for 30 min at room temperature for complex formation. CRs were calculated theoretically, taking into account the net charge of the peptide and net charge of pDNA at pH 7.

For *in vivo* studies 20 μg of pLuc2 per animal (0.8 mg/kg) was mixed with 1 mM peptide at CR 2 or CR4 in MQ water and the volume of complexes was kept constantly at 150 μl. For PEGylated complexes, first NF-PEG was mixed with pDNA in MQ water and incubated for 5 min followed by addition of parent NF. After 30 min of incubation 50 μl of 20% glucose was added to preformed complexes and immediately injected intravenously *via* tail vein.

2.5. Complex stability assay

The formation of NF/pDNA complexes was verified by electrophoresis on 1% agarose gel. For that 3 μl of loading dye was added to the preformed complexes before running the gel.

In heparin displacement assay NF/pDNA complexes were mixed with PicoGreen reagent (1:150) (Invitrogen) and incubated for 10 min at room temperature. Thereafter heparin sulfate (Sigma-Aldrich) over the range of concentrations from 0.25 to 10 mg of salt was added to 1 ml of complex solution and incubated 30 min at 37 °C. In each experiment naked DNA stained with PicoGreen was used to normalize the PicoGreen signal detected from the complexes. After this fluorescence was analyzed using a fluorescence plate reader, Fluostar Optima (BMG Labtech, Aylesbury, United Kingdom).

2.6. Proteinase K assay

Proteinase K treatment was carried out in order to evaluate the stability of preformed NF/pDNA complexes to enzymatic degradation of CPP by proteinases. Pre-formed complex solution with either pDNA (0.05 μg per sample) or MQ was transferred to a black 96-well plate and 90 μl of MQ water was added. After a short period of mixing, fluorescent DNA intercalating dye dilution was added (Quant-iT™ PicoGreen®, ThermoFisher Scientific) and incubated for 5 min at RT. The fluorescence was measured (Synergy MX, BioTek; $λ_{ex}$ 492 and $λ_{em}$ 535) to quantify the initial accessibility of pDNA. Thereafter, 20 μl of Proteinase K (~20 mg/ml, >600 U/ml, Thermo Scientific) was mixed with 1 ml of MQ and 10 μl of this solution was transferred to each well and incubated for 10 min at 26 °C. Fluorescence was measured over a period of 2 h at 26 °C. These readings were normalized to free pDNA and MQ fluorescence and expressed as the digestion time required to release 50% of the pDNA from NF/pDNA complexes.

2.7. Cell culture

HeLa, U87-MG, N2A and HT1080 cells were grown in Dulbecco's modified Eagles medium (DMEM). Medium was supplemented with glutamax, 0.1 mM non-essential amino acids, 1.0 mM sodium pyruvate, 10% fetal bovine serum (FBS), 100 U/ml penicillin, and 100 mg/ml streptomycin (PAA Laboratories GmbH, Germany).

2.8. Cell viability test

Cell viability was analyzed by CytoTox-Glo™ Assay (Promega, Sweden). 10,000 HeLa cells were seeded into 96-well plates 24 h before the experiment. Complexes were formed as described or peptide solution in MQ was made 10× of given concentration. 100 μl of serum-containing medium was added to cells. 24 h after treatment the number of dead cells and total cells was measured on the GLOMAX™ 96 microplate luminometer. Results are given as % of living cells (viability).

2.9. Plasmid transfection in vitro

50,000 HeLa or U87-MG cells were seeded 24 h before the experiment into 24-well plates. For gene expression measurements cells were treated with NF and luciferase encoding plasmid complexes,

which were prepared as described above, for 4 h in serum-containing medium. Lipofectamine™ 2000 (Invitrogen, Sweden) was used according to the manufacturer's protocols. After 4 h, 1 ml of full growth media was added and incubated for 20 h. Then cells were washed twice with phosphate buffered saline (PBS), and lysed using 100 µl 0.1% Triton X-100 in PBS buffer for 30 min at +4 °C. Luciferase activity was measured in relative light units (RLU) using Promega's luciferase assay system on GLOMAX™ 96 microplate luminometer (Promega, Sweden). Data was normalized to protein content measured with DC protein determination kit (Bio-Rad Laboratories, Inc., USA).

For FACS experiments GFP encoding plasmid (EGFP) or cy5-labled plasmid were mixed with NFs for complex formation. After treatment of U87-MG cells with complexes for indicated periods of time, cells were rinsed with PBS, detached from the plate with Trypsin in PBS for 5 min at 37 °C and suspended in PBS containing 5% FBS. FACS analysis was carried out with a BD LSR II flow cytometer (BD Biosciences, USA) equipped with a 488 nm argon laser. Population of viable cells was determined from a scatter plot: forward scattered light vs. side scattered light. A minimum of 10,000 events from the viable cells population per sample were analyzed. Acquired data was analyzed with BD FACS Diva Software.

For estimation of NF55/p-Luc2 stability complexes were prepared as in vivo nanoparticles as described below. Thereafter, complexes were lyophilized and stored 7 days at room temperature. Next, lyophilized particles were dissolved in MQ and their transfection ability in HeLa cells were compared to freshly prepared in vivo complexes. Plasmid transfection experiment and luciferase activity was measured and analyzed as described below.

2.10. Biodistribution study

The pDNA was labeled using Label IT® Cy™5 Labeling Kit according to manufacturer protocol (Mirus, USA). 20 µg of Cy5-labeled pDNA was mixed with NF55 at CR4 and after 40 min. of incubation glucose was added and complexes were immediately injected i.v. via tail vein.

As a control 20 µg of uncomplexed Cy5-labeled pDNA was administered. The biodistribution of Cy5-pDNA and NF55/Cy5-pDNA comlexes was evaluated at different time points - 0,5 h, 1 h, 3 h and 24 h. For that, mice ($n = 2$) were imaged in vivo using IVIS Lumina II (CaliperLS, USA). Cy-5 fluorescence values were acquired form region of interest (ROIs) representing lungs, liver, bladder, brain and tumor.

2.11. In vivo gene delivery

Gene expression levels were evaluated post mortem 24 h after injecting NF/pDNA complexes i.v. into tail vein. We have previously shown that 24 h time point is optimal for p-CMV-Luc2 [24]. For the gene delivery studies, male and female BALB/c (8 week old) were used.

The mouse Neuro2a tumors were induced in BALB/c mice subcutaneously. Human tumor xenografts (intracranial U87MG and subcutaneous HT-1080) were induced in nude animals (Hsd:Athymic Nude-Foxn1nu female, 4–6 week old, Harlan, UK). The xenografting was performed by implanting the cell suspension subcutaneously to the left flank or intracranially into one of the striatums (stereotaxic coordinates A = +1, L = +2, V = +3). The s.c. tumors were induced by resuspending 1×10^6 cells in 100 µl volume of ice-cold DMEM without any supplements. For intracranial tumor induction, anesthetized mice were injected with 1×10^6 cells in 5 µl of DMEM without any supplements. A mixture of 75 mg/kg ketamine (Bioketan, Vetoquinol, France) and 1 mg/kg dexmedetomidine (Dorbene, Laboratorios SYVA, Spain) i.p in saline was used for the anesthesia. After surgery, the anesthesia was blocked using the α2-adrenergic antagonist atipamezole hydrochloride (Antisedan, Pfizer), 1 mg/kg s.c. Postoperation analgesia was achieved with meloxicam 0.5 mg/kg, buprenorphine 0.1 mg/kg, s.c. once a day for 3 days postop. At the appearance of the first signs of tumor growth (for the subcutaneous tumors, tumor size of approx 100 mm3; for the intracranial tumors, the first sign is usually weight loss, sometimes

motor deficiencies), mice were injected i.v. (via tail vein) with the NF/pDNA complexes (formed as described in complex formation section). Each animal received a single 200 µl i.v. injection of 20 µg pDNA, formulated with NFs at CR2 or CR4. After 24 h mice were sacrificed using cervical dislocation and whole organs were harvested and snap-frozen on dry ice. The organs were homogenized and analyzed as described previously [24]. For in vivo-JetPEI or TurboFect in vivo Transfection Reagent we used 20 µg or 50 µg pDNA according to the manufacturer's protocols. All animal experiments and procedures were approved by the Estonian Laboratory Animal Ethics Committee (approvals no 81, dated Apr 04, 2016, and 69 and 70, dated Feb 9, 2011).

2.12. Transmission electron microscopy (TEM)

For the morphological characterization of NF55/pDNA or lyophilized NF55/pDNA nanocomplexes a negative staining TEM analysis was performed as described before [25]. Briefly, copper grids were covered with formvar film and with carbon layer using Leica EM ACE600 carbon coater (Leica Microsystems, Germany). Then, 10 µl of each sample were applied onto grids for 1 min, followed by washing with Milli-Q water. Thereafter, samples were exposed to 2% aqueous uranyl acetate solution for 1 min. Next, the excess of stain was removed with filter paper and the samples were allowed to air-dry. The specimens were imaged at 120 kV accelerating voltage using FEI Tecnai G2 Spirit transmission electron microscope (FEI, The Netherlands). Freshly prepared or lyophilized NF55/pDNA nanocomplexes were formed at CR4 (peptide over nucleic acid) as described above.

3. Results and discussion

3.1. Optimization of charge and secondary amphipathicity leads to enhanced transfection efficacy

We recently designed a series of CPPs that we term NickFects (NF), which are based on a stearylated TP10, also known as PF3. These peptides are able to efficiently transfect various cell lines with plasmid DNA (pDNA), siRNA, and splice-correcting oligonucleotides [9,11,26]. The two most effective NF vectors for pDNA delivery were found to be NF1 and NF51. NF1 contains a phosphorylated Tyr in the third position and Ile11 is replaced with Thr as compared to stearylated TP10 sequence. In NF51 Lys7 is replaced with Orn and the δ-amino group of Orn is used for the subsequent synthesis instead of ordinarily used α-NH2 group in order to gain a kinked structure [10,11]. Characterization of the physiochemical properties of these NF nanoparticles revealed that NF51 condenses DNA into homogeneous and more stable nanoparticles and promotes better escape of nanoparticles from endosomal compartments compared to NF1 [10]. However, because the biological activity of pDNA delivered with NF1 was on the same level as NF51, we hypothesized that the negatively charged phosphoryl group in the backbone of NF1 may work to improve transfection. In order to utilize the advantages of both peptides, namely the branch in NF51 and the negative charge in NF1, we designed a new series of NFs (Table 1).

Firstly, we tested if the efficacy of NF1 and its analogue NF2 are actually due to the negative charge provided by the phosphoryl group in the backbone, which reduces the overall net charge of the peptide from +4 to +3. For this, we replaced the negatively charged phosphoryl groups on Tyr3 and Thr8 in the NF1 and NF2 sequences, respectively, with a Glu residue that is also negatively charged at physiological pH. This demonstrate that neither of these modifications proved to be deleterious and both of the new analogues, NF16 and NF17, displayed similar transfection efficacies compared with their parent peptide (Fig. 1A).

Thereafter, we accomplished similar alterations in the backbone of NF51 thereby providing NF18 and NF19. These novel peptides have a net charge of +3, while their parent peptide NF51 has +4. However, the pDNA transfection results were surprising because NF18 was over 300 times less effective than NF51 (Fig. 1A) and NF19 was almost at

Table 1
Sequences of NickFect peptides.

Peptide	Sequence	Charge	Ref
NF1	Stearyl-AGY(**PO₃**)LLGKTNLKALAALAKKIL-$_{NH2}$	+3	[26]
NF2	Stearyl-AGYLLGKT(**PO₃**)NLKALAALAKKIL-$_{NH2}$	+3	[26]
PF3	Stearyl-AGYLLGKINLKALAALAKKIL-$_{NH2}$	+4	[12]
NF16	Stearyl-AG**E**LLGKTNLKALAALAKKIL-$_{NH2}$	+3	
NF17	Stearyl-AGYLLGK**E**NLKALAALAKKIL-$_{NH2}$	+3	
NF18	(Stearyl-AG**E**LLG)δ-**O**INLKALAALAKKIL-$_{NH2}$	+3	
NF19	(Stearyl-AGYLLG)δ-**OE**NLKALAALAKKIL-$_{NH2}$	+3	
NF51	(Stearyl-AGYLLG)δ-**O**INLKALAALAKKIL-$_{NH2}$	+4	[11]
NF54	(Stearyl-AGYLLG)δ-**O**INLKALAALAA**K**IL-$_{NH2}$	+3	
NF55	(Stearyl-AGYLLG)δ-**O**INLKALAALAKA**I**L-$_{NH2}$	+3	
NF551	(Stearyl-AGYLLG)δ-**O**INLK**A**K(C^a)AALA**K**AIL-$_{NH2}$	+3	
NF552	(Stearyl-AGYLLG)δ-**O**INL**K**LALAALAKAILC^a-$_{NH2}$	+3	

Different modifications which were introduced in parent peptide PF3 sequence are indicated with bold font.

^{a} PEG2000-Cys is conjugated *via* disulphide bond.

the same level, being only three-fold less effective than NF51. Comparison of NF18 and NF19 showed that insertion of extra negative charge towards C-terminus was more relevant. We continued by modifying the C-terminal part of the peptide that is essentially a mastoparan sequence from wasp venom. Since the addition of extra negative charge did not improve the efficacy of the novel analogues, we decided to reduce number of positively charged lysines in the backbone instead of inserting extra negative charge. We designed a new NF51 analogue, NF54, where the total net charge of the peptide was reduced by replacing a positively charged Lys18 with Ala. Similarly to NF19, the transfection efficacy of NF54 was lower than NF51. Further on we proceeded to modify the secondary amphibithicity of the peptide. We designed NF55 with reduced net charge and distinct hydrophilic region on α-helical wheel projection (Fig. 1S). *In vitro* pDNA transfection proved the importance of secondary amphipathicity as NF55 resulted in two-fold higher gene expression level than NF51 (Fig. 1A). To further prove the NF55 utilization as efficient transfection regent we showed the NF55 efficiency in various cell lines (Fig. 1 and Fig. S7) and in primary cells (Fig. S8) and gene modification in biologically relevant context, outside reporter system (Fig. S9).

3.2. CD and computational methods confirm enhanced secondary amphipathicity of NF55

To verify that the new modifications change the secondary structure of the peptide, we utilized circular dichroism spectroscopy (CD). The CD curves of all NFs that we tested displayed characteristic features of an α-helical structure with a typical curve shape and minima at 208 and 222 nm (Fig. 2A).

However, the CD spectra of NF55 in a water based solution revealed that the modification in its chemical structure results in an increase in its helicity. This data shows that NF55 has a higher percentage of α-helix in its secondary structure than the other peptides (Fig. 2B). Using a K2D2 secondary structure estimate from the CD spectra data we found that NF55 contains 57% of an α-helix structure. Although both NF51 and NF54 have α-helical structures in water, the percentage of α- helicity is significantly lower at 38% and 28%, respectively (Fig. 2B). Interestingly, the parent peptide, PF3 (that has non-branched backbone structure), revealed only slight helicity under these test conditions, thereby proving that all of the alterations that have been performed on NF peptides previously have worked to increase the percentage of α-helix secondary structure.

Next, we characterized these analogues by calculating their molecular surfaces, molecular electrostatic potentials (MEP), and hydrophilic/hydrophobic maps (Fig. 2C). NF55 had MEP and hydrophilic/hydrophobic maps that resemble those of NF51 more than those of NF54. In particular, the NF55 and NF51 maps have three regions of negative electrostatic value (colored blue) in a staircase manner on the same side of the alpha helix (Fig. 2C). Neither NF54 nor PF3 have this feature. These results suggest that NF55 presents a distinct signature of three negative electrostatic regions in close vicinity and aligned on the same face of the peptide at regular intervals.

NF51 has small values for both helix and beta propensity to interact, as calculated by statistical mechanics algorithm Tango for the residues: ALAAL. NF54, on the other hand, had a quite large propensity to interact and more available residues: ALAALAA. NF55 has moderate values for this interaction propensity and fewer residues: ALAALA. Even if individual peptide alpha-helicity follows the trend NF55 > NF51 > NF54, and this correlates with efficiency, the propensity for interaction is NF54 (3.72) > NF55 (1.86) > NF51 (0.58). This may contribute to a better understanding of the mechanism of association of each peptide into peptide multimers. The interaction propensity of the peptides was calculated based on the sequences using force-fields and a statistical analysis using various databases. For these peptides, the difference in their carbon tails would not be apparent, because they only consider standard amino acid residues. It seems from our CD and Tango results, that NF54 has a higher amount of beta strand than NF51 or NF55, and that this may induce a larger degree of aggregation.
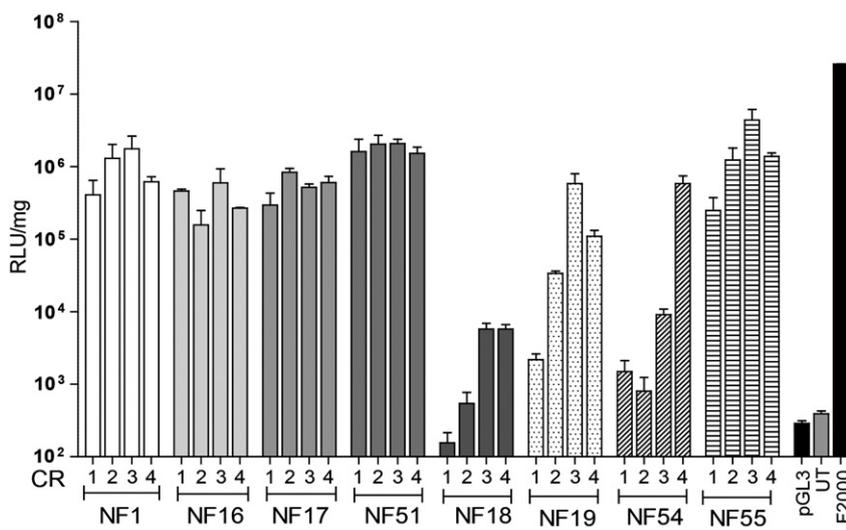
Fig. 1. Luciferase-encoding plasmid transfection efficacy of NFs in Hela cells at different charge ratios. Untreated cells (UT) were used as negative control and Lipofectamine™ 2000 (LF2000) as a positive control. The data is presented as mean ± SEM (*n* = 3).
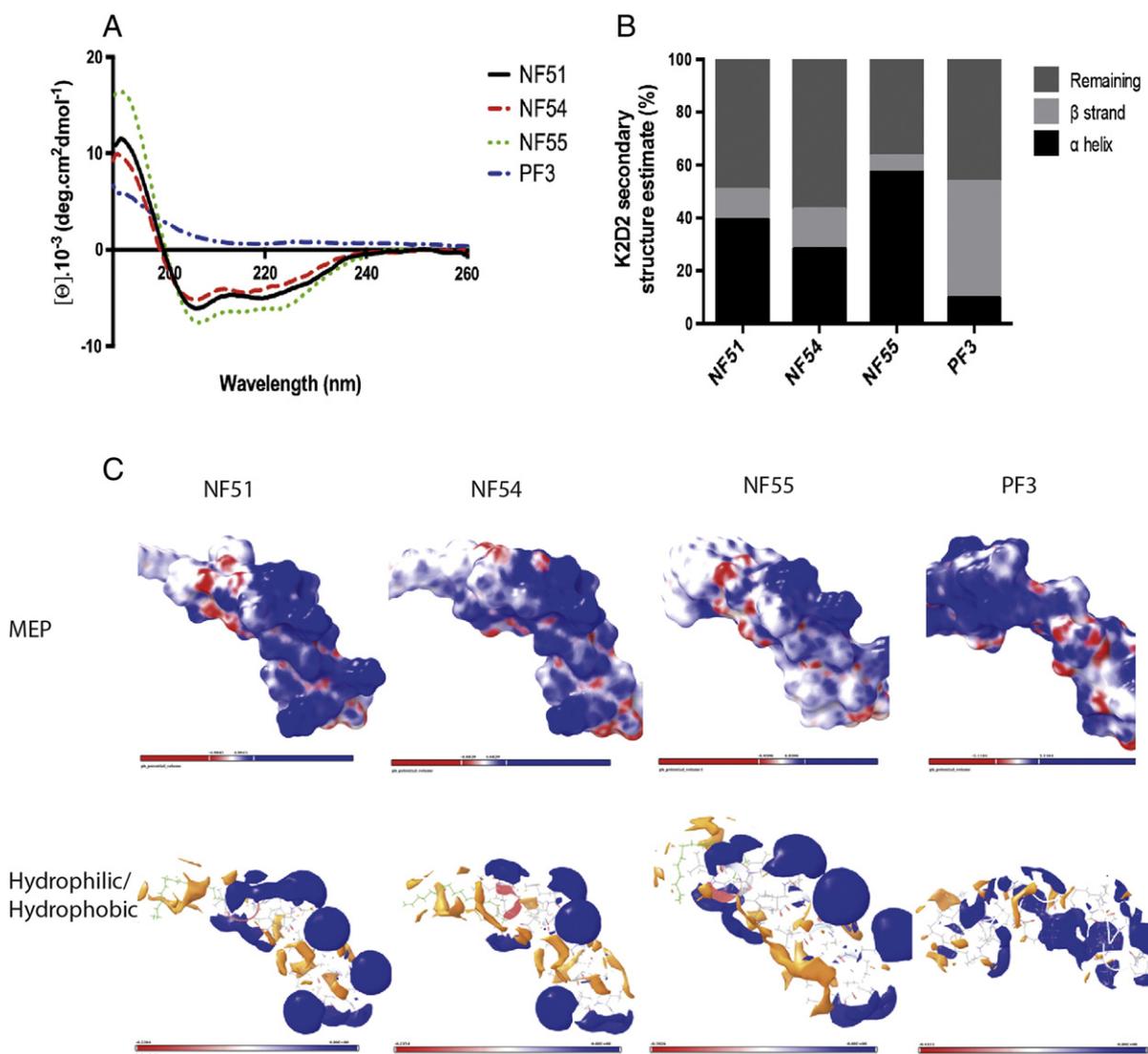
Fig. 2. CD spectra of peptides in Milli-Q water at 20 °C (A). K2D2 algorithm was used to estimate the relative abundance of α-helical and β-sheet conformation in the peptides (B). The MEP figures show regions of the molecular surface that are negative electrostatic (towards the color blue), positive electrostatic (towards the color red), or neutral (white). The hydrophilic/hydrophobic maps show regions that are either hydrophilic (colored in blue), or where a hydrophobic partner would have a favorable interaction (colored in orange) (C).

3.3. Better endosomal escape enables to transfect larger cell population

An important parameter of any efficient delivery vector is its ability to carry cargo into the majority of cells in a large cell population. To investigate the ability of NF to transfect a large cell population, we estimated the number of cells that express pDNA after treatment with NF/EGFP encoding plasmid complexes (Fig. 3A). After a single treatment, NF55 transfected cells in a concentration dependent manner, peaking at CR4 and then plateauing, while NF51 demonstrated less variance between the different charge ratios.(Fig. 3A). Although all peptides were able to deliver pDNA into the majority of cells as shown by transfecting Cy5-labled pDNA, a large fraction of the cell population did not express the transfected reporter gene (Fig. S4). This indicates that the delivered nucleic acids may not reach to the nucleus.

Endosomal entrapment is a major bottleneck in many cellular delivery methodologies, including CPP-mediated delivery [27,28]. Because NF/pDNA nanoparticles utilize an endocytic pathway, they often remain trapped inside endocytic organelles within cells and fail to reach the cytosolic space of cells efficiently [4]. Therefore, we used co-treatment with chloroquine (CQ) in order to investigate whether the differences in uptake into the cells and gene expression were caused by the entrapment of NF/pDNA nanoparticles within endosomal compartments. CQ neutralizes the acidic pH of endocytotic vesicles and promotes the release of entrapped nanoparticles from intracellular vesicles [29,30]. Treatment with CQ (Fig. 3B) revealed that NF55, in contrast with NF51, is not significantly hindered by endosomal entrapment. We may speculate that this is caused by the more pronounced secondary amphipathic nature of the NF55 peptide. NF51 displays increased transfection in the presence of CQ, which indicates that the higher uptake potential of NF51 is hindered by endosomal entrapment and does not translate into higher rates of transfection.

The results obtained from *in vitro* experiments demonstrate that the novel peptide, NF55 is a more effective delivery vector for pDNA than NF51. The CD analysis we performed shows that NF55 has the highest percentage of α- helix secondary structure compared with the other peptides we tested. This increased helicity may contribute to better transfection through improved membrane interaction, specifically, through improved endosomal escape. Furthermore, NF54, which has positive charges not localized on one side of the helical wheel, has a lower transfection capacity. Previous studies have suggested that the
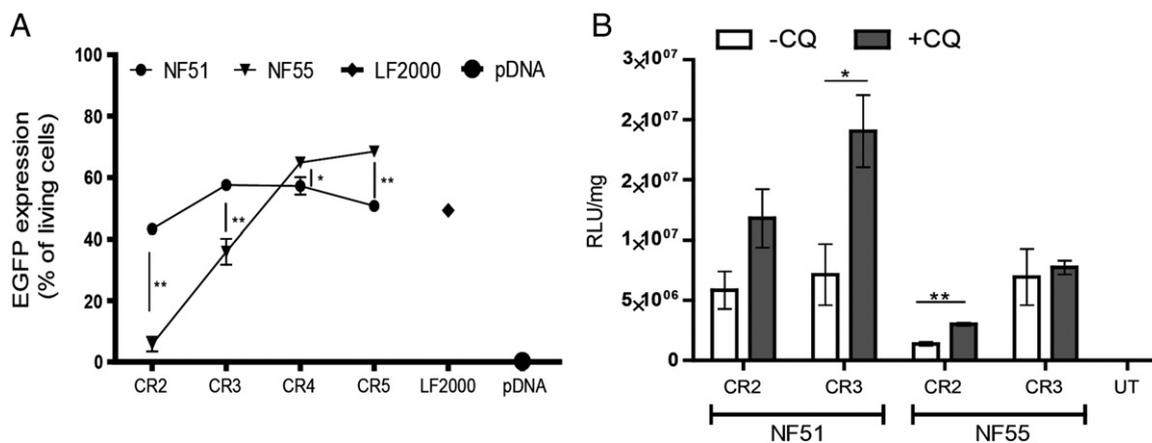
Fig. 3. Flow cytometry analysis showing NF51 and NF55 transfected pDNA gene expression in cell population. U87-MG cells were transfected with GFP encoding plasmid/NF nanoparticles and analyzed after 24 h (A). NFs transfection efficacy with CQ co-treatment (B). The data is presented as mean ± SEM ($n = 3$), $^*P < 0.05$; $^{**}P < 0.01$ (Student t-test, two-tailed distribution, two-sample unequal variance (heteroscedastic)).

structural conformation of peptides may influence their interaction with lipid membranes and thereby enhance their ability to penetrate cells [18]. A correlation between the helical character of peptides and pDNA transfection has been found before by Niidome et al. [31]. Furthermore, disruption of the helicity of the parent peptide TP10 has been shown to decrease its cell penetrating activity [19].

NF55/pDNA particles were able to transfect a larger fraction of the cell population and shuttle more pDNA into the nucleus thereby inducing higher reporter gene expression than NF51. Furthermore, NF55 particles displayed only a minor improvement in pDNA delivery after CQ treatment, which suggests better endosomal escape than NF51 particles.

3.4. NF55 forms stable particles with pDNA

We verified that NF peptides are able to form nanoparticles with pDNA using agarose gel electrophoresis (Fig. S6).

To investigate the stability of NF/pDNA nanoparticles, we treated the complexes with a growing gradient of a competitor molecule, heparin, and measured the amount of liberated pDNA. Contrary to our expectations, the heparin displacement assay indicates that NF51 forms significantly more labile nanoparticles than NF54 and NF55 (Table 2 and Fig. S2A). At 5.7 mg/ml of heparin, half of the pDNA was dissociated from NF51/pDNA nanoparticles, while NF54 and NF55 both required a higher concentration of heparin to dissociate pDNA from their nanoparticles. We found that both NF54 and NF55 have IC50 values around 7.1 mg/ml (Table 2). Data from the displacement assay indicates that reducing the net charge of the peptide does not reduce the stability of the nanoparticles that form, indicating that the cationic charge is not the only factor needed to form efficient nanoparticles for transfection. This phenomenon has also been observed by others. Previous studies have demonstrated that hydrophobic peptides bind more strongly to DNA. [31] The increased hydrophobicity of NF54 and NF55 compared to NF51 (Table 2) might explain why the nanoparticles from these

Table 2
Characterization of physicochemical properties of NF/pDNA nanoparticles.

Peptide	Charge	IC50(mg/ml)	Stability to Proteinase K treatment (min)	logP	Ref
NF51	+4	5.7	37.7	4.82	[11]
NF54	+3	7.1	7.7	4.95	
NF55	+3	7.1	73.9	4.95	

IC50 values were calculated for heparin ability to displace DNA from NF nanoparticles.
NF/pDNA nanoparticles resistance to Proteinase K treatment was examined and time for reaching 50% of nanoparticle dissociation was calculated.
MarvinSketch64 was used to calculate logP values.

peptides display greater stability because increased hydrophobicity results in stronger hydrophobic interactions with pDNA.

The stability of nanoparticles in serum is critical to their use in drug delivery *in vivo*. To characterize the stability of NF55/pDNA particles in serum-like environment we studied the resistance of these particles to Proteinase K digestion. NF55 provided the highest resistance to protease digestion with 50% of the pDNA accessible after 74 min of enzymatic incubation (Table 2 and Fig. S2B). NF54 nanoparticles have less resistance to protease treatment. Already after eight minutes of incubation, half of the NF54 particles dissociated, while 37 min of incubation was necessary to dissociate half of the NF51 particles. Thus, NF55/pDNA nanoparticles have an increased half-life in a serum-like environment compared with their parent peptide. We may assume that the distinct hydrophilic/hydrophobic regions in NF55 condense pDNA into more compact nanoparticles that offer better protection from proteinase digestion.

3.5. NF55 is an efficient in vivo transfection reagent

Based on the results of *in vitro* assays, we chose the most potent peptide, NF55, for *in vivo* testing. First, we studied the biodistribution of NF55/Cy5-labled pDNA (Fig. S5). NF55/pDNA nanoparticles were detected mostly in tumor tissue, peaking at 3 h after injection and then gradually declining. After 3 h, 15-fold higher fluorescence signal in tumor were detected compared with pDNA treatment. After 24 h, high Cy5 fluorescence signal in bladder indicated that the nanoparticles accumulated into the renal tissue.

Thereafter, we compared both the transfection efficiency and specificity of NF51 and NF55 *in vivo*. NF55/pDNA treated animals exhibited significantly higher gene induction than mice treated with NF51/pDNA nanoparticles (Fig. 4A). As often reported with cationic particles we observed notable reporter gene expression in lungs and liver [32]. Intrestingly we also observed 22-fold higher bioactivity in the cerebellum and seven-fold higher bioactivity in the rest of the brain after NF55/pDNA treatment compared to naked pDNA. NF51/pDNA treated animals we mainly detected reporter gene expression in liver, yet it remained in the same range as naked pDNA treatment by providing only a ten-fold improvement. Although *in vitro* tests revealed that NF55 particles provide only a two-fold higher gene transfection efficacy compared with NF51 particles, *in vivo* results demonstrate significantly improved gene delivery. This indicates that the secondary amphipathicity of this peptide is important for *in vivo* gene delivery. NF55/pDNA nanoparticles provide comparable expression in the main organs and over five-fold greater bioactivity in cerebellum compared with a commercially available *in vivo* transfection reagents, *in vivo*-JetPEI and Turbofect. The measured luminescence in lung tissue was over two-fold lower. Compared with NF55 and JetPEI, TurboFect was

Fig. 4. NF51 and NF55 pDNA transfection in balb/c mice at CR4. 20 μg pDNA was used to form nanoparticles with different delivery vectors except TurboFect termed with *, where 50 μg pDNA was used (A). Transfection efficacy of NFs in nude mice bearing intracranial U87-MG tumor at CR4 (B). NF55 and NF55 PEGylated peptide pDNA transfection in mice bearing s.c N2A tumors at CR2 (C) and in mice bearing s.c HT1080 tumors at CR4 (D). Legends in C and D graph show the percentage of PEGylated peptide added to NF55/pDNA particles. The ability of NF/pDNA complexes to induce gene expression levels in different tissues was evaluated in vivo. Complexes with 20 μg or 50 μg of pLuc2 plasmid were administered i.v. via the tail vein. After 24 h, luciferase activity was measured and normalized to the protein content. Values are represented as fold increase of RLU/mg over the pDNA treated group. The data is from at least three representative experiments performed in triplicate, presented as mean ± SEM, *$P < 0.05$; **$P < 0.01$ (Student t-test, two-tailed distribution, two-sample unequal variance (heteroscedastic)).

not effective at 20 μg pDNA, although higher concentration of pDNA (50 μg) yielded in similar efficiencies as seen with NF55 and JetPEI.

Because NF55/pDNA particles provide high reporter gene expression in brain, but especially in cerebellum, we continued our in vivo studies using a mouse intracranial brain tumor model which we used to assess the gene induction efficacy of NF/pDNA nanoparticles. Curiously, we observed a 45-fold increase in gene expression in tumor-containing striatum (Fig. 4B). Despite this significant accumulation in tumor tissue, similarly high gene expression was also detected in unaffected brain regions. This indicates that although high tumor gene induction may be achieved with NF55, more elaborate modifications to add targeting mechanism may be needed [24]. In addition, a high luminescence signal was also detected in both lungs and liver. Notable reporter gene expression was also observed in NF51/pDNA treated animals, however, the gene expression remained lower in all tissues compared with NF55/pDNA treatment.

These findings demonstrate that in comparison with NF51, NF55 displays only a slight improvement in transfection in vitro, yet provides significantly better transfection efficacy in vivo. In addition to secondary

amhipathicity, NF55 has a stronger interaction with pDNA (Table 2 and Fig. S2A) and provides improved resistance to protease digestion (Table 2 and Fig. S2B). These properties can explain why NF55 particles result in more transfection. The stability of nanoparticles in serum is important for their use in drug delivery where intravenous injection could result in nanoparticle disassembly and degradation.

3.6. PEGylation of NF55 enhances pDNA transfection into tumor tissue

As mentioned before, additional targeting modifications may be needed to achieve efficient tumor targeting. In the current report, as a starting point, we utilized one simple approach to enhance passive accumulation to tumors. We utilized the steric shielding effect of polyethylene glycol (PEG) to improve the half-life in serum and reduce renal clearance of the NF55 nanoparticles. In solid tumors, the extracellular pH is much lower and the intracellular glutathione concentration is significantly higher than in normal tissues. Therefore, pH- and glutathione-sensitive disulphide bonds can facilitate the delivery of pDNA specifically into tumor cells [33].

Various analogues of PEGylated NF55 were designed to find a PEGylation site that maximizes the α-helicity of the peptide. These analogues were analyzed by CD spectroscopy (Table S2). Two such analogues, NF551 and NF552, demonstrated the highest percentage of α-helix secondary structure and were chosen for application *in vivo*. NF551 was PEGylated orthogonally by replacing 13th Leu with Lys and adding an extra Cys. We PEGylated NF552 C-terminally by adding an extra Cys. We attached a PEG2000 to each NF55 *via* a disulphide-bond (Table 1). Complex formation with PEGylated peptides was performed as described previously [24]. Different PEGylation rates were achieved by mixing NF55, pDNA and PEGylated NF55, by substituting a proportion of the parent peptide with PEGylated analogue.

We moved away from the intracranial model and continued our studies using a subcutaneous tumor model to screen for various formulations. Again, NF55 provided good pDNA transfection in tumors, with a 62-fold increase in reporter gene expression (Fig. 4C). Addition of either 10% or 20% NF551 to NF55/pDNA particles increased the tumor accumulation two-fold. Interestingly, this also raised the rate of lung transfection. The lung-to-tumor ratio did not decrease with either a 10% or 20% NF551 peptide nanoparticle treatment (Fig. 4C). Because orthogonally PEGylated NF551 failed to reduce lung accumulation we tried C-terminally PEGylated NF552.

The addition of NF552 significantly reduced lung accumulation from 9000-fold (0% of NF552) to 125 fold- (50% of NF552) compared with naked pDNA treatment (Fig. 4D). The orthogonally PEGylated peptide showed a modest reduction in lung transfection compared with the C-terminally modified peptide. The most efficient nanoparticle formulation we found was 20% NF552 with NF55/pDNA particles. This formulation increases nanoparticles tumor accumulation over three times and reduces lung transfection over 38-fold compared with NF55/pDNA treatment alone.

Finally, we analyzed potential side effects of the treatment with NF55/pDNA particles. Injection of either NF55 or JetPEI complexes with pDNA similarly elevated liver enzymes at 24 h (Table S1), compared to the injection of naked pDNA. Investigation of the H&E stained tissue slices revealed no pathological changes in liver in case of NF55/pDNA particles (data not shown). However, administration of JetPEI/pDNA resulted in characteristic perivascular inflammatory infiltration and necrosis, as is common for polyethyleneimine and nucleic acid complexes [32]. No pathological changes were found in lung tissues either for NF55 or JetPEI complexes.

In agreement with other reports, the addition of a PEGylated peptide enhances tumor accumulation and decreases dose-dependent lung transfection [34]. The PEGylation site within the NF55 sequence was also found to be important because NF552 significantly reduced lung transfection in comparison with NF551.

3.7. NF55/pDNA solid dispersion formulation is stable

Finally, we studied the solid dispersion formulation of NF55/pDNA particles. We formed nanocomplexes of NF55 and pDNA in a 5% of glycose solution as used for *in vivo* experiments and examined their size and morphology with TEM analysis (Fig. 5B). NF55 packed the pDNA into small nanoparticles that typically had a spherical or elliptic shape and a diameter of between 50 and 150 nm. Occasionally, smaller particles associated with each other and formed larger (d ≤ 300 nm) conglomerates with an irregular shape. Next, we assessed whether NF55/pDNA nanocomplexes are also able to retain their small size and morphology after drying and storage. We lyophilized pre-formed NF55/pDNA complexes containing glucose and stored them at room temperature for one week. Thereafter, we dissolved the complexes in Milli-Q and performed TEM analysis. We found that lyophilization of NF55/pDNA nanocomplexes did not markedly affect their shape. Importantly, the nanocomplexes did not aggregate after lyophilization and storage at room temperature, and their size was similar to that of non-lyophilized nanocomplexes. Thereafter, we used stored lyophilized complexes (containing glucose) for *in vitro* transfection experiments. There was no statistically significant difference in transfection efficiencies compared with freshly prepared nanoparticles (Fig. 5A). This result proves that lyophilized NF55/pDNA nanoparticles can be stored at room temperature for at least 7 days without losing their biological activity. These NF55/pDNA particles demonstrate an excellent stability profile without further additives or special storage conditions. The stability of NF55/pDNA solid formulation is very important for its further development into a therapeutic product. In general, solid formulations are
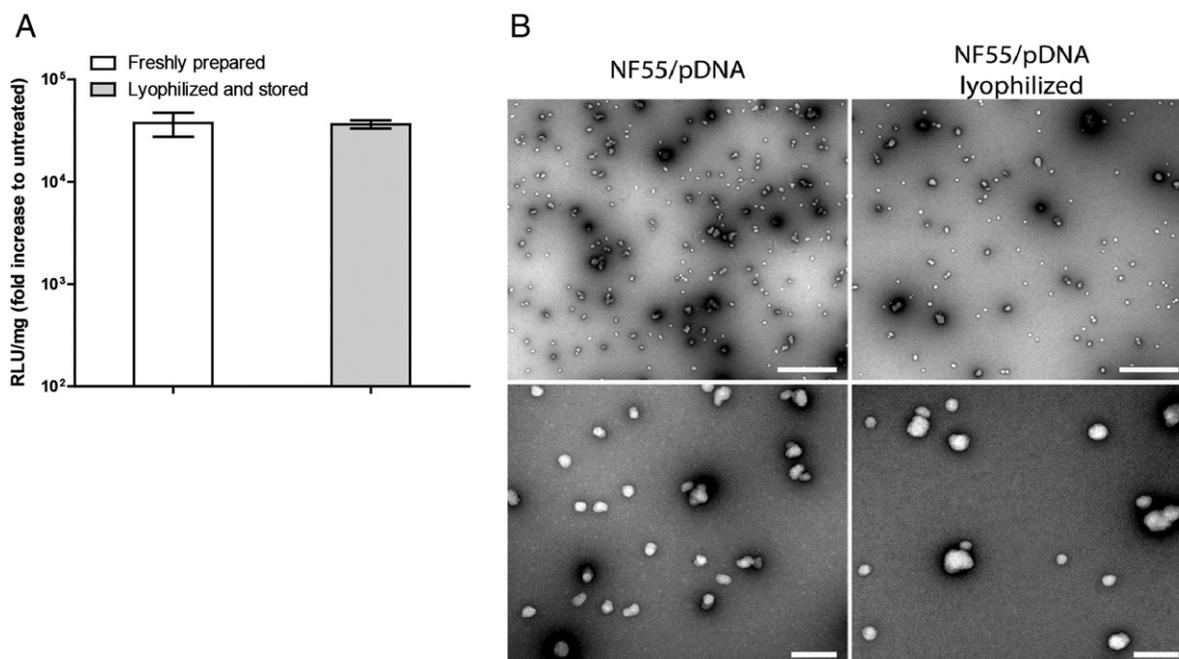
Fig. 5. NF55/pDNA complex stability. Freshly prepared NF55/pDNA *in vivo* complexes or lyophilized and stored (7 days) complexes bioactivity in Hela cells. The data is presented as mean ± SEM (*n* = 3) (A). Freshly prepared NF55/pDNA nanocomplexes in 5% glycose solution (left panels). NF55/pDNA nanocomplexes after lyophilization and storage at RT for 7 days reconstituted in water (right panels). Scale bars: 1 μm (top); 200 nm (bottom) (B).

easier to handle, are stable during storage and transportation, and remain the most widely used pharmaceutical formulation [35].

4. Conclusions

In conclusion, we have rationally designed by modifying the net charge and the amphipathicity of the CPP an efficient *in vivo* gene delivery vector. NF55 conveyed pDNA into tumor tissues in mice bearing intracranial or s.c tumors. The reporter gene expression of NF55/pDNA particles in tumor increased even further after addition of PEGylated NF55. This demonstrates that the addition of active targeting molecules could further increase tumor tissue targeting. These results indicate the potential of NF55 for tumor-targeting delivery of therapeutic nucleic acids.

Conflicts of interest

None of the authors have any conflicts of interest to disclose.

Acknowledgments

Appendix A. Supplementary data

Supplementary data to this article can be found online at http://dx.doi.org/10.1016/j.jconrel.2016.09.022.

References

[1] H. Yin, et al., Non-viral vectors for gene-based therapy, Nat. Rev. Genet. 15 (2014) 541–555.
[2] S.R. Husain, J. Han, P. Au, K. Shannon, R.K. Puri, Gene therapy for cancer: regulatory considerations for approval, Cancer Gene Ther. 22 (2015) 554–563.
[3] R.L. Juliano, The delivery of therapeutic oligonucleotides, Nucleic Acids Res. gkw236 (2016), http://dx.doi.org/10.1093/nar/gkw236.
[4] H. Margus, K. Padari, M. Pooga, Cell-penetrating peptides as versatile vehicles for oligonucleotide delivery, Mol. Ther. 20 (2012) 525–533.
[5] J. Jo, S. Hong, W.Y. Choi, D.R. Lee, Cell-penetrating peptide (CPP)-conjugated proteins is an efficient tool for manipulation of human mesenchymal stromal cells, Sci. Rep. 4 (2014).
[6] Q. Zhang, H. Gao, Q. He, Taming cell penetrating peptides: never too old to teach old dogs new tricks, Mol. Pharm. 12 (2015) 3105–3118.
[7] A.B. Hill, M. Chen, C.-K. Chen, B.A. Pfeifer, C.H. Jones, Overcoming gene-delivery hurdles: physiological considerations for nonviral vectors, Trends Biotechnol. 34 (2016) 91–105.
[8] J. Suhorutsenko, et al., Cell-penetrating peptides, PepFects, show no evidence of toxicity and immunogenicity in vitro and in vivo, Bioconjug. Chem. 22 (2011) 2255–2262.
[9] P. Arukuusk, L. Pärnaste, M. Hällbrink, Ü. Langel, PepFects and NickFects for the intracellular delivery of nucleic acids, Methods Mol. Biol. Clifton NJ 1324 (2015) 303–315.
[10] P. Arukuusk, et al., Differential endosomal pathways for radically modified peptide vectors, Bioconjug. Chem. 24 (2013) 1721–1732.
[11] P. Arukuusk, et al., New generation of efficient peptide-based vectors, NickFects, for the delivery of nucleic acids, Biochim. Biophys. Acta 1828 (2013) 1365–1373.
[12] M. Mäe, et al., A stearylated CPP for delivery of splice correcting oligonucleotides using a non-covalent co-incubation strategy, J. Control. Release 134 (2009) 221–227.
[13] U. Soomets, et al., Deletion analogues of transportan, Biochim. Biophys. Acta Biomembr. 1467 (2000) 165–176.
[14] C.M. Dunkin, A. Pokorny, P.F. Almeida, H.-S. Lee, Molecular dynamics studies of transportan 10 (Tp10) interacting with a POPC lipid bilayer, J. Phys. Chem. B 115 (2011) 1188–1198.
[15] R. Sharma, S. Shivpuri, A. Anand, A. Kulshreshtha, M. Ganguli, Insight into the role of physicochemical parameters in a novel series of amphipathic peptides for efficient DNA delivery, Mol. Pharm. 10 (2013) 2588–2600.
[16] Rajpal, A. Mann, R. Khanduri, R.J. Naik, M. Ganguli, Structural rearrangements and chemical modifications in known cell penetrating peptide strongly enhance DNA delivery efficiency, J. Control. Release Off. J. Control. Release Soc. 157 (2012) 260–271.
[17] K. Rittner, et al., New basic membrane-destabilizing peptides for plasmid-based gene delivery in vitro and in vivo, Mol. Ther. 5 (2002) 104–114.
[18] A. Ziegler, Thermodynamic studies and binding mechanisms of cell-penetrating peptides with lipids and glycosaminoglycans, Adv. Drug Deliv. Rev. 60 (2008) 580–597.
[19] J. Song, et al., Cellular uptake of transportan 10 and its analogs in live cells: selectivity and structure–activity relationship studies, Peptides 32 (2011) 1934–1941.
[20] A.T. García-Sosa, I. Tulp, K. Langel, U. Langel, Peptide-ligand binding modeling of siRNA with cell-penetrating peptides, Biomed. Res. Int. 2014 (e257040) (2014).
[21] Schrödinger Software Package version 2015.
[22] A.-M. Fernandez-Escamilla, F. Rousseau, J. Schymkowitz, L. Serrano, Prediction of sequence-dependent and mutational effects on the aggregation of peptides and proteins, Nat. Biotechnol. 22 (2004) 1302–1306.
[23] C. Perez-Iratxeta, M.A. Andrade-Navarro, K2D2: estimation of protein secondary structure from circular dichroism spectra, BMC Struct. Biol. 8 (2008) 25.
[24] K.-L. Veiman, et al., PEG shielded MMP sensitive CPPs for efficient and tumor specific gene delivery in vivo, J. Control. Release 209 (2015) 238–247.
[25] H. Margus, P. Arukuusk, Ü. Langel, M. Pooga, Characteristics of cell-penetrating peptide/nucleic acid nanoparticles, Mol. Pharm. 13 (2016) 172–179.
[26] N. Oskolkov, et al., NickFects, phosphorylated derivatives of transportan 10 for cellular delivery of oligonucleotides, Int. J. Pept. Res. Ther. 17 (2011) 147–157.
[27] I. Nakase, et al., Cellular uptake of arginine-rich peptides: roles for macropinocytosis and actin rearrangement, Mol. Ther. 10 (2004) 1011–1022.
[28] I.M. Kaplan, J.S. Wadia, S.F. Dowdy, Cationic TAT peptide transduction domain enters cells by macropinocytosis, J. Control. Release 102 (2005) 247–253.
[29] M. Zenke, et al., Receptor-mediated endocytosis of transferrin-polycation conjugates: an efficient way to introduce DNA into hematopoietic cells, Proc. Natl. Acad. Sci. U. S. A. 87 (1990) 3655–3659.
[30] P. Midoux, et al., Specific gene transfer mediated by lactosylated poly-L-lysine into hepatoma cells, Nucleic Acids Res. 21 (1993) 871–878.
[31] T. Niidome, et al., Binding of cationic α-helical peptides to plasmid DNA and their Gene transfer abilities into cells, J. Biol. Chem. 272 (1997) 15307–15312.
[32] P. Chollet, M.C. Favrot, A. Hurbin, J.-L. Coll, Side-effects of a systemic injection of linear polyethylenimine-DNA complexes, J. Gene Med. 4 (2002) 84–91.
[33] L. Liu, P. Liu, Synthesis strategies for disulfide bond-containing polymer-based drug delivery system for reduction-responsive controlled release, Front. Mater. Sci. 9 (2015) 211–226.
[34] M.L. Immordino, F. Dosio, L. Cattel, Stealth liposomes: review of the basic science, rationale, and clinical applications, existing and potential, Int. J. Nanomedicine 1 (2006) 297–315.
[35] K. Ezzat, et al., Solid formulation of cell-penetrating peptide nanocomplexes with siRNA and their stability in simulated gastric conditions, J. Control. Release 162 (2012) 1–8.